

Hierarchical Model Validation of the Falx Cerebri and Tentorium Cerebelli

A. J. Golman, A. C. Wickwire, T. P. Harrigan,
A. S. Iwaskiw, R. S. Armiger, A.C Merkle

Applied Physics Laboratory, The Johns Hopkins University

This paper has not been screened for accuracy nor refereed by any body of scientific peers and should not be referenced in the open literature.

ABSTRACT

The falx cerebri and tentorium cerebelli are extensions of the dura mater that divide the hemispheres of the brain and separate the cerebellum from the occipital lobe. These structures support the brain and are therefore included in most human head finite element models (FEMs). However, the material properties and response of these structures have not been previously investigated. The objective of this study was to use a hierarchical validation approach to experimentally characterize the falx cerebri and tentorium cerebelli at both tissue and component levels and then to use this data to validate a falx and tentorium FEM. First, component level indentation tests were conducted on four Post Mortem Human Subjects (PMHS) to characterize the in-situ medial-lateral stiffness across the falx cerebri. The non-linear response was characterized in two piece-wise linear segments resulting in stiffness of 0.45 ± 0.41 to 1.49 ± 0.51 N/mm for the “toe” (0-1N) and “loaded” (1-3N) phases, respectively. Second, tissue level uniaxial tension tests were performed on dogbone samples die-cut from the falx cerebri and tentorium cerebelli of six PMHS to characterize the stress-strain relationship. The mean modulus was 36 ± 25 MPa with a thickness of 0.41 ± 0.16 mm. The experimental data was then used to determine the optimal pretension value and validate the response in a computational model. Indentation tests were simulated at six similar locations between the PMHS and FEM using the mean experimental modulus of 36 MPa. The optimal pretension was found to be 0.1% strain. Additionally, the modulus and pretension were perturbed from the optimal values to characterize parameter sensitivity. Compared to the simulation response when using previously referenced material properties, this parameter combination reduced the average error by 74%. The modulus, pretension, and thickness parameters for falx cerebri and tentorium cerebelli are hierarchically validated here for application in human head FEMs.

INTRODUCTION

The falx cerebri and tentorium cerebelli are extensions of the dura mater that divide the hemispheres of the brain and separate the cerebellum from the occipital lobe. During a dynamic impact event, the falx cerebri is frequently attributed to having an effect on the stress-strain response of the brain (Hardy et al., 2007; Margulies et al., 1990; Yoganandan et al., 2009). Under coronal rotational acceleration, using a baboon physical head model, the falx was shown to considerably reduce the strains in the brain (Margulies et al., 1990). In terms of brain and skull relative motion, the falx was discussed as a potential structure responsible for brain motion lag in coronal plane impacts (Hardy et al., 2007). Additionally, the falx was thought to be the source for smaller relative motion during coronal rotation compared to sagittal rotation (Kleiven and Hardy, 2002). The proximity to the falx was also shown to influence the brain motion patterns for impacts in the coronal and transverse planes, however the significance of this response was concluded to be unknown (Hardy et al., 2007).

The falx and tentorium have been modelled structurally in multiple head finite element models (FEMs) (Chafi et al., 2010; Ho and Kleiven, 2009; Kimpara et al., 2006; Kleiven and Hardy, 2002; Takhounts et al., 2008, 2003; Yang et al., 2011; Zhang et al., 2001). While the falx was included in all of these FEMs, only one study directly investigated the effects of the falx on brain response (Li et al., 2007). Using a simplified two-dimensional FEM to simulate coronal rotational accelerations, the flexibility of the falx was shown to have an effect on regional brain strains, thus motivating the importance of using accurate material properties (Li et al., 2007). However, the falx and tentorium material properties for the aforementioned head FEMs were all derived from dura mater experimental tests (Table 1), and the *in situ* response has not been previously verified.

Most of the head FEMs use a linear elastic material model with modulus of 31.5 MPa to represent the dura, falx, and tentorium. This modulus was taken from the storage modulus value ($E_1 = 4570 \text{ psi} = 31.5 \text{ MPa}$) from free vibration tests performed on human dura (Galford and McElhaney, 1970). Different from the majority of head FEMs, Ho and Kleiven (2009) used a nominal stress-strain relationship, rather than a simple linear elastic model, derived from human dura mater uniaxial tension tests (van Noort et al., 1981). Despite the different material models used, all of these head FEMs used material properties derived from tests performed on dura mater rather than the falx/tentorium structures. Takhounts et al. (2008) attributed some of the error of their head FEM response to the lack of material properties data for the falx and tentorium and suggested that they should be characterized in the future.

The objective of this study was to use a hierarchical approach (Henninger et al., 2010; Oberkampf et al., 2004) to validate a falx and tentorium FEM by leveraging the material properties extracted from tissue coupon tests and the *in situ* medial-lateral force-deflection response from component indentation tests.

Table 1: Falx and tentorium material properties used by previous head FEMs.

Head FEM Reference	Density (kg/m ³)	Material Constants	Poisson's Ratio	Thickness (mm)
Zhou 1995	1133	E = 31.5 MPa	0.45	N.R.
Zhang 2001	N.R.	N.R.	N.R.	N.R.
Kleiven 2002	1130	E = 31.5 MPa	0.45	N.R.
Takhounts 2003	N.R.	E = 31.5 MPa	0.45	7
Kimpara 2006	1133	E = 31.5 MPa	0.45	1
Takhounts 2008	1133	E = 31.5 MPa	0.45	N.R.
Ho 2009	1130	Stress-Strain	N/A	N.R.
Chafi 2010	1133	E = 31.5 MPa	0.45	N.R.

N.R. = Not Reported

EXPERIMENTAL METHODS

Specimen

The post mortem human surrogates (PMHS) used for this study were obtained from the Maryland State Anatomy Board (Table 2). Experiments were performed to characterize the falx-tentorium response at both the tissue and component levels using these subjects. The specimen preparation for each test protocol is described in the corresponding sections below.

Component Level in-situ Indentation Tests

Component level indentation tests were conducted on four PMHS to characterize the *in-situ* medial-lateral stiffness across the falx cerebri (Figure 1). Two offset sagittal osteotomies allowed removal of the cerebral hemispheres, while maintaining the structural attachment regions to the skull (Figure 2). Indentation locations were identified by mapping a 10 mm grid onto the membrane surface. Prior to indentation, the skull was rigidly attached to a table. The load-deflection response was then characterized by quasi-statically indenting various locations in the medial-lateral direction at 1, 2 and 3 N (sub-failure loads) for a total of 149 indentation tests across all specimens. An 8821S Instron with a 2527 series Dynacell was used for performing these tests.

Tissue Level Uniaxial Tension Tests

To characterize the falx and tentorium at the tissue level, the cranial membranes were excised after completing the indentation testing. Dog-bone shaped coupons of 34.8 mm length were created using an ASTM D638 die at multiple orientations and were then tested under uniaxial tension on a TA Instruments RSA-G2 dynamic mechanical analysis testing machine (Figure 3). Dog-bone samples were oriented to be parallel, perpendicular, and at an oblique angle to the primary direction of tensile load. Low- and mid-rate (0.01 mm/sec and 10 mm/sec, respectively) tests were performed to only 3% elongation in order to prevent permanent tissue deformation. Higher-rate tests were conducted at 100 mm/sec and tested to failure. All tests were conducted in a fluid-filled chamber that was elevated to approximately physiological temperature. Elastic modulus was the primary output analyzed from these tests and compared between multiple groups by performing a one-way ANOVA and then breaking down into individual pairwise t-tests with a Bonferroni correction factor ($p < 0.01$ was considered significant).

Table 2: Specimen information.

Specimen	Race	Cause of Death	Age (years)	Mass (kg)	Height (cm)	L1-L4 BMD (g/cm^2)	# of Indentation Locations	# of Tension Coupons
A	Caucasian	Lung cancer	56	136	182	1.138	24	11
B	Caucasian	Lung cancer	69	69	175	1.054	45	19
C	Caucasian	Lung cancer	68	104	188	1.314	40	15
D	Caucasian	Hypertension	58	113	178	1.366	40	16
E	Caucasian	Liver cancer	63	90.7	175	1.168	N/A	23
F	Caucasian	Stomach cancer	53	77	183	1.096	N/A	15

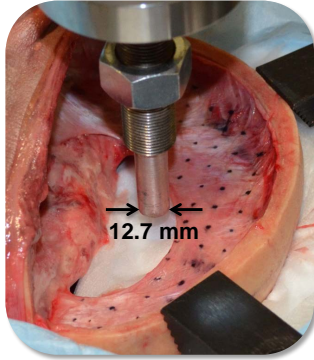


Figure 1: Indentation test configuration.

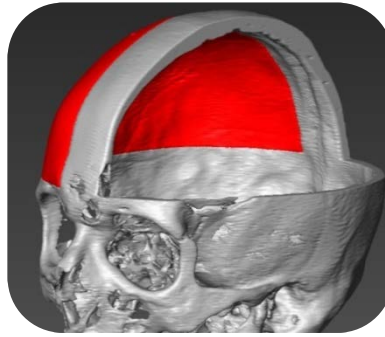


Figure 2: Schematic of the offset sagittal osteotomies.

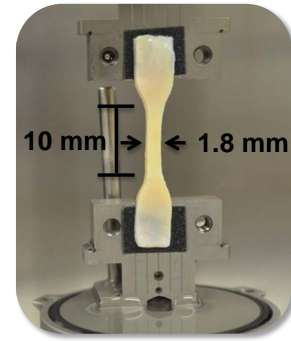


Figure 3: Tension test preparation.

EXPERIMENTAL RESULTS & DISCUSSION

Component Level *in-situ* Indentation Tests

The minimum indentation stiffness was located mid-brain nearest the corpus callosum and the maximum stiffness was located in the posterior aspect adjacent to the skull. The stiffness varied from 0.45 ± 0.41 to 1.49 ± 0.51 N/mm for toe and loaded phases, respectively (Table 3). Toe and loaded stiffness responses were significantly different ($p < 0.001$), confirming that there were at least two distinct phases in the indentation response. Higher order (greater than 2) piece-wise fits were omitted from this analysis for simplicity.

For both the toe and loaded regions, the force-displacement stiffness response was similar across specimen. Specimen D was observed to have a lower average stiffness in the loaded region; however this difference was not statistically significant. This difference could also be seen from the scatter plots (Figure 4) and summary statistics (Table 3). The only statistically significant inter-specimen difference was the 62% difference in stiffness during the toe-phase between Specimen D and B.

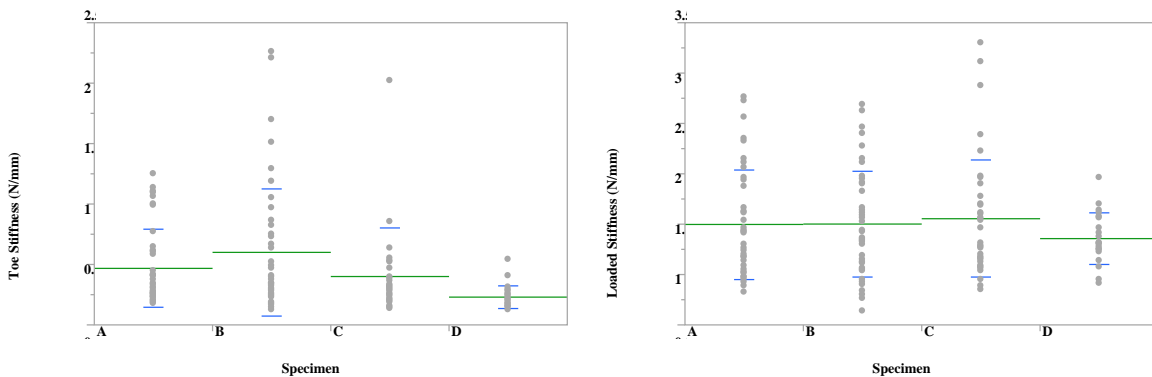


Figure 4: Indentation test scatter plots of toe region (left) and loaded region (right) stiffness by specimen. Legend: green bar = mean; blue bars = standard deviation.

Table 3: Indentation stiffness summary statistics.

	Toe Stiffness (N/mm)					Loaded Stiffness (N/mm)				
	All	A	B	C	D	All	A	B	C	D
mean	0.45	0.47	0.60	0.40	0.23	1.49	1.50	1.50	1.55	1.36
std dev	0.41	0.32	0.52	0.41	0.09	0.51	0.54	0.53	0.58	0.25
upper 95%	0.52	0.57	0.76	0.53	0.27	1.58	1.67	1.66	1.74	1.47
lower 95%	0.38	0.36	0.44	0.27	0.19	1.41	1.32	1.34	1.37	1.25

Stiffness during the loaded region of the response curves was location dependent, with higher stiffness near the skull attachment (Figure 5). Mechanically, the edge of the falx near the skull represents a fixed boundary, whereas the edge near the corpus callosum represents an unsupported free boundary. This location dependency was captured using two different linear regression models to predict loaded stiffness. The first regression model contains the distance from the skull (Eq. 1) and the second included an additional term for distance from the corpus callosum (Eq. 2). The r^2 value ranged 0.25-0.54 and 0.5-0.87 for the specimen and was 0.34 and 0.63 for all data combined for model 1 and 2, respectively (Table 4).

$$\text{Model 1: } \text{Stiff}_{\text{load}} = b_0 + b_1 d_{\text{skull}} \quad (\text{Eq. 1})$$

$$\text{Model 2: } \text{Stiff}_{\text{load}} = b_0 + b_1 d_{\text{skull}} + b_2 d_{\text{corpus}} + b_3 d_{\text{skull}} d_{\text{corpus}} \quad (\text{Eq. 2})$$

Where d_{skull} and d_{corpus} are the distance from the indentation point to the skull and corpus callosum, respectively and $b_{0,1,2,3}$ are the regression model coefficients.

Including the corpus callosum distance, in addition to the distance from the skull, accounts for the regional differences in the model and substantially increased the fit of the regression model (Table 4). For example, in the posterior falx the corpus callosum distance was larger for a given skull distance compared to the middle and anterior portions of the falx. One potential method to improve the regression fit of model 2 is to include an additional term that quantifies the regional effect of the stiffness. However, this additional term was chosen to not be included due to the large specimen geometry differences between each specimen. Model 2 adequately predicts the loaded stiffness given the distances between two important structures: the skull and corpus callosum (Figure 6).

Table 4: Regression model r^2 values for loaded stiffness. Model 1 includes skull distance (Eq. 1) and model 2 includes both skull distance and corpus callosum distance (Eq. 2).

Specimen	r^2	
	Model 1	Model 2
A	0.54	0.87
B	0.38	0.57
C	0.25	0.64
D	0.52	0.74
All data combined	0.34	0.63

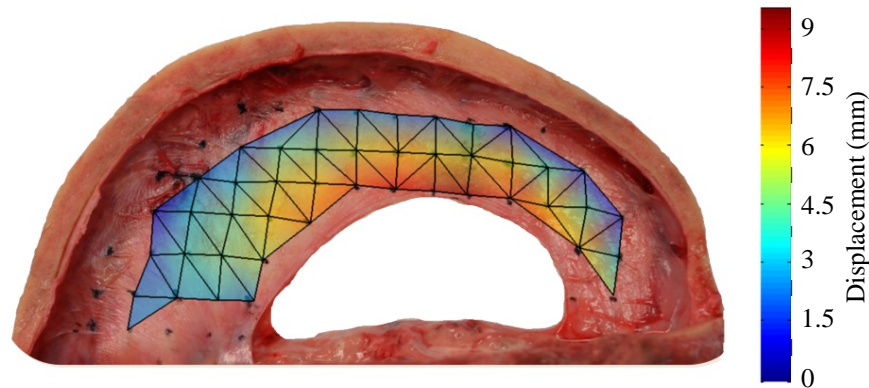


Figure 5: Contour plot representing the displacement during a 3 N indentation of Specimen C.

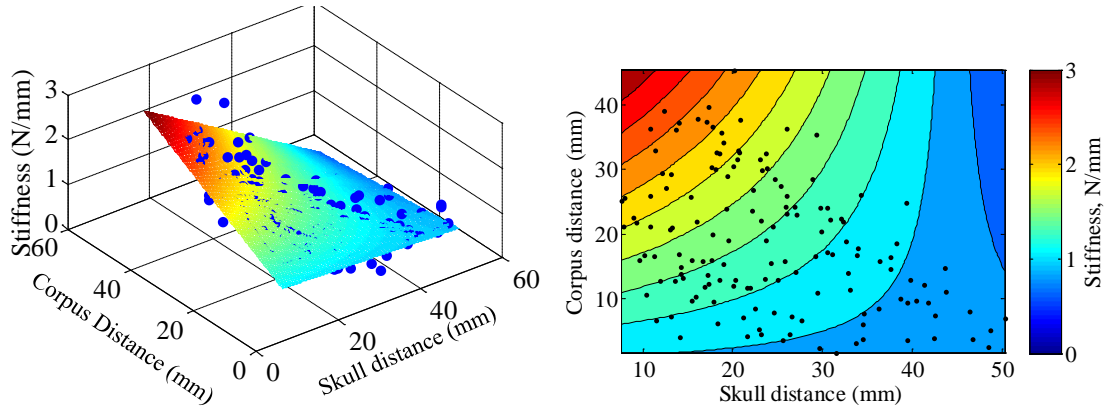


Figure 6: Model 2 Multiple linear regression model fit $r^2=0.63$.

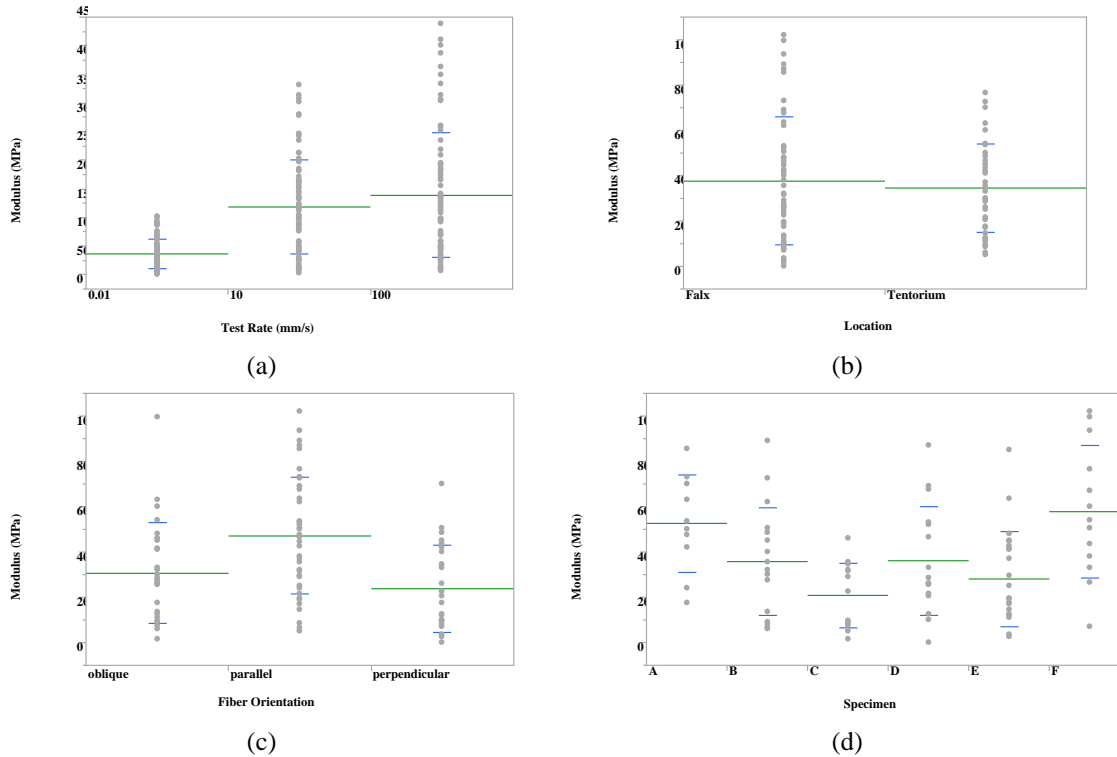


Figure 7: Modulus comparison by test rate (a) and for the 0.01 mm/s test rate location (b), fiber orientation (c), and specimen (d). Legend: green bar = mean; blue bars = standard deviation.

Tissue Level Uniaxial Tension Tests

Across the 270 uniaxial tension tests, no significant difference was observed between the modulus of the falx and that of the tentorium (Figure 7b). However, a significant difference was detected between the falx (0.45 ± 0.16 mm) and tentorium (0.36 ± 0.15 mm) thicknesses. Combined, the mean thickness was 0.41 ± 0.16 mm. The modulus for 0.01 mm/s quasi-static tests (36 ± 25 MPa) was significantly less than the dynamic 10 mm/s (118 ± 82 MPa) and 100 mm/s (138 ± 109 MPa) tests (Figure 7a). The large standard deviations in the modulus data can be attributed to the differences in fiber orientation for each uniaxial specimen (Figure 7c), which had a statistically significant effect on modulus for every test rate, with the largest difference between parallel and perpendicular fiber orientations. Per ANOVA, some significant specimen differences existed for the quasistatic modulus (Figure 7d). The mean quasi-static modulus of 36 MPa in this study agrees well with the 31.5 MPa storage modulus from previous dura mater free vibrations tests (Galford and McElhaney, 1970).

COMPUTATIONAL MODELING METHODS

Finite Element Model

The geometry of the falx and tentorium was derived from the surfaces of the Johns Hopkins University Applied Physics Laboratory human head FEM (Roberts et al., 2012) using Hypermesh (Altair Engineering Inc., Troy, MI) and then parametrically meshed with 2 mm long quadrilateral shell elements using True-Grid (Scientific Applications Inc., Livermore, CA) (Figure 8). The falx was assumed to be homogenous, linear-elastic, and isotropic despite differences in modulus due to fiber orientation. To account for these differences, the average quasi-static modulus for all orientations (36 MPa) was used as reference point for the FEM. The mean experimental thickness of 0.41 mm was used for the FEM shell thickness.

A linear elastic material model was used to represent the falx and tentorium tissue. In order to create pretension within the falx and tentorium, a thermal model was added. By decreasing the numerical temperature, the mesh would contract and because the falx and tentorium is fixed to the skull, pretension was created. This numerical temperature was held constant throughout the simulation and was not intended to represent physiological temperature. The pretension value was inversely optimized using the *in-situ* component level indentation tests.

Finite Element Model Validation

The indentation simulations were set up to replicate the experimental tests (Figure 8). Similar to the experimental tests, indentation points were selected by overlaying a 10 mm grid onto the falx FEM. The quasi-static indentation of the 12.7 mm diameter indenter was simulated using LS-DYNA (Livermore Software Technology Corporation, Livermore, CA) until the contact force exceeded 4 N. The displacements at 0, 1, 2, and 3 N were then extracted to compare to the experimental results. The quasi-static indentation simulation was assumed to be no different than the multistep experimental tests which used load control to determine the displacements at each load level.

To inversely determine the optimal pretension, six similar indentation points were chosen to compare between the FEM and PMHS (Figure 8). The FEM and PMHS indentation deflection response was compared at each location for 1 and 3 N with pretension varying between 0 and 1.0%. The validation metric (ϕ) represents the average standard deviation from the experimental mean deflections at 1 and 3 N (Eq 3)

$$\phi = \frac{1}{2} \left(\frac{1}{n} \sum_{i=1}^n \left| \frac{\mu_{1N} - FEM_{i,1N}}{\sigma_{1N}} \right| + \frac{1}{n} \sum_{i=1}^n \left| \frac{\mu_{3N} - FEM_{i,3N}}{\sigma_{3N}} \right| \right) \quad (\text{Eq. 3})$$

where n is the number of indentation location points compared between the FEM and experiments (for pretension determination, n=6).

After determining the optimal pretension value, parametric simulations were performed to fully explore the parameter space and the effects on ϕ . For this parameter study, the FEM modulus was varied from 11 to 86 MPa (12.5 MPa increments) and pretension from 0 to 1.0% strain (0.1% increments) for a total of 77 simulations. Then, the simulation with the optimal model parameters was compared to the simulation results using parameters found in the literature (31.5 MPa modulus and 1 mm thickness).

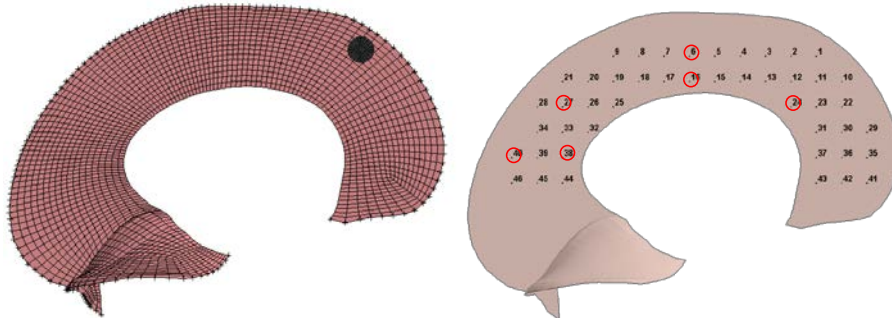


Figure 8: Falx-tentorium FEM with fixed outer edges representing the skull attachment (left). All 44 indentation points simulated with the six indentation points (red circles) chosen for PMHS comparison.

COMPUTATIONAL MODELING RESULTS & DISCUSSION

The optimal pretension was found to be 0.1% strain which corresponded to an average error of 0.85 (Figure 9) compared to an average error of 3.31 using previous literature parameters for the falx and tentorium FEM (Figure 10). Therefore, the parameters determined using this hierarchical approach reduced the average error by 74%.

Sensitivity study results over a modulus ranging from 11 to 86 MPa and pretension from 0 to 1.0% resulted in a banded region within the parameter space that best matches the experimental data (Figure 11). For lower modulus values, higher levels of pretension were required to best match the experimental data. The opposite was true for high modulus values, where little to no pretension was required for a good match. This inverse linear correlation between pretension and modulus to match the experimental data is likely related to the contribution of these parameters towards the effective stiffness of the tissue's response. In order to achieve the necessary effective stiffness, either the modulus needed to be sufficiently high or pretension needed to be added.

Within this best-fit region, the global minimum occurred at 36 MPa and 0.1% pretension (Figure 11). This parameter combination was the same as found from performing inverse optimization to determine the optimal pretension given the mean experimental modulus (Figure 9). Considering the wide parameter space explored and the homogeneous isotropic assumptions made, the optimal parameter combination was found using the mean experimental modulus of 36 MPa. Following the hierarchical approach for model development and validation (Henninger et al., 2010; Oberkampff et al., 2004), the mean experimental modulus from the tissue level tests (36 MPa) with the pretension inversely determined from the component level tests (0.1%) should be considered for future head finite element models.

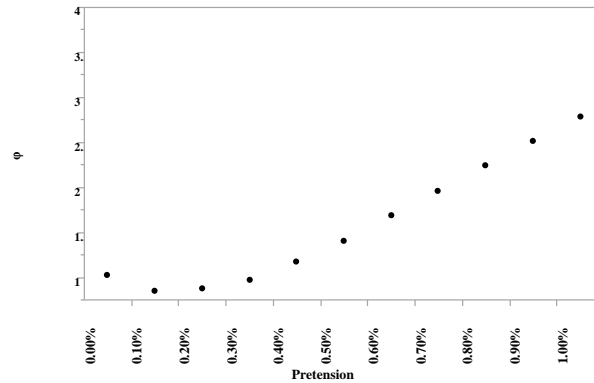


Figure 9: Validation metric ϕ for a modulus of 36 MPa and pretension ranging from 0% to 1% strain. The minimum (0.85) occurs at 0.1% strain.

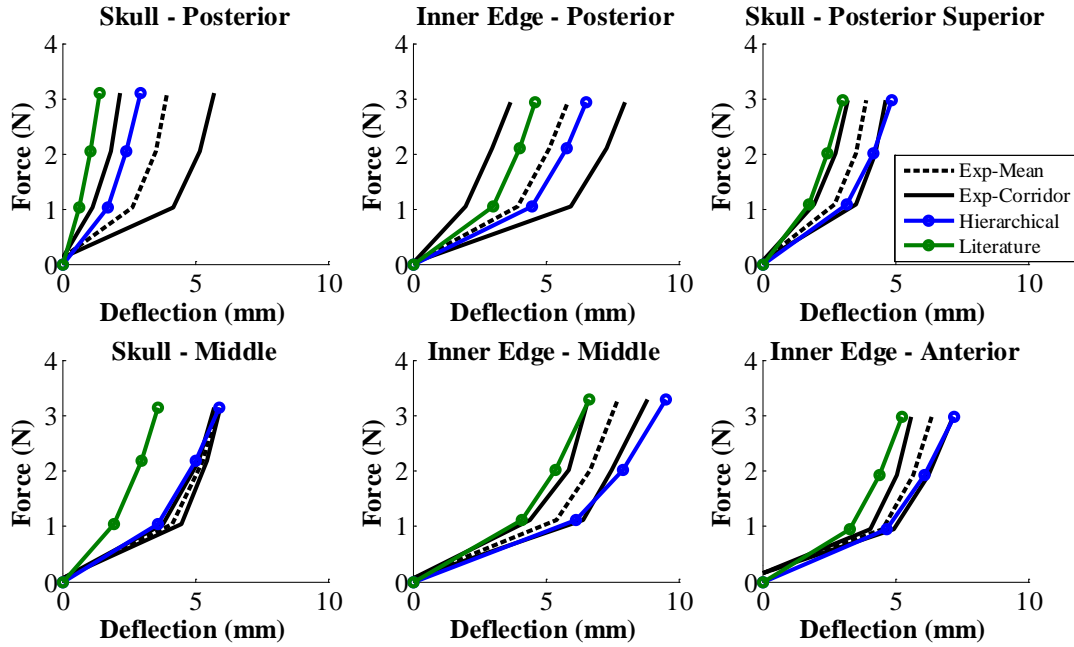


Figure 10: Force-deflection comparison between FEM and PMHS at the six indentation points. The parameters for the hierarchical FEM were $E=36$ MPa, pretension=0.1%, and thickness = 0.41 mm and the literature parameters were $E=31.5$ MPa, pretension=0%, and thickness = 1 mm.

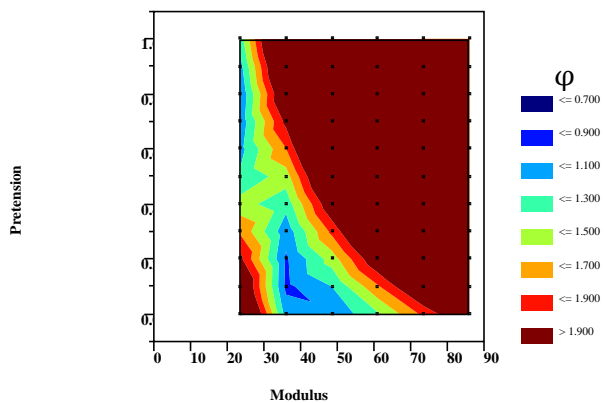


Figure 11: Contour plot of the validation metric ϕ , representing the average number of standard deviations the FEM differs from the experimental data for a given pretension and modulus parameter combination. Each grid location represents a simulation parameter combination. Note that the results from simulations with a modulus of 11 MPa were not shown due to instabilities in the model.

CONCLUSION

The objective of this study was to develop a hierarchically validated falx cerebri and tentorium cerebelli FEM. First, the falx and tentorium were experimentally characterized at both tissue and component levels using uniaxial tension tests and *in-situ* indentation tests. Then, the indentation tests were simulated and a parametric study was performed by varying elastic modulus and pretension to minimize the error between the FEM response and PMHS tests. This parameter study resulted in the mean experimental modulus of 36 MPa and 0.1% pretension to be the optimal parameter combination which resulted in a reduction of error by 74% compared to the response when using literature values.

One limitation of this model is that the geometry of each PHMS specimen varied, however the experimental results were compared to a single computational model of the cranium. Future work will focus on matching the geometry on a subject specific basis by warping the existing mesh for each specimen (Figure 12) to compare each indentation point between FEM and PMHS. This comparison will allow for the evaluation of error associated with the optimal material properties ($E=36$ MPa, pretension=0.1%, thickness=0.41 mm) derived from this study. The results from this study can be used to improve the biofidelity of the falx cerebri and tentorium cerebelli in future head FEMs.

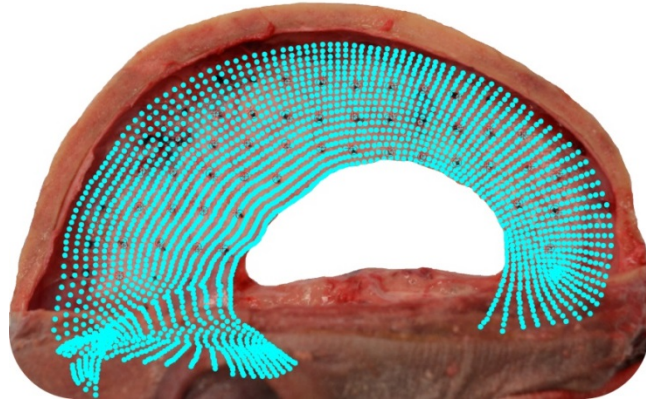


Figure 12: Falx and tentorium FEM mesh (light blue) warped to match PMHS.

ACKNOWLEDGEMENTS

The authors would like to acknowledge the United States Army Medical Research Acquisition Activity for supporting this research effort.

REFERENCES

- CHAFI, M.S., KARAMI, G., ZIEJEWSKI, M., 2010. Biomechanical assessment of brain dynamic responses due to blast pressure waves. *Ann. Biomed. Eng.* 38, 490–504.
- GALFORD, J.E., MCELHANEY, J.H., 1970. A viscoelastic study of scalp, brain, and dura. *J. Biomech.* 3, 211–21.
- HARDY, W.H., MASON, M.J., FOSTER, C.D., SHAH, C.S., KOPACZ, J.M., YANG, K.H., KING, A.I., BISHOP, J., BEY, M., ANDERST, W., TASHMAN, S., 2007. A Study of the Response of the Human Cadaver Head to Impact 51, 17–80.
- HENNINGER, H.B., REESE, S.P., ANDERSON, A E., WEISS, J. a, 2010. Validation of computational models in biomechanics. *Proc. Inst. Mech. Eng. Part H J. Eng. Med.* 224, 801–812.
- HO, J., KLEIVEN, S., 2009. Can sulci protect the brain from traumatic injury? *J. Biomech.* 42, 2074–80.
- KIMPARA, H., NAKAHIRA, Y., IWAMOTO, M., MIKI, K., ICHIHARA, K., KAWANO, S., TAGUCHI, T., 2006. Investigation of anteroposterior head-neck responses during severe frontal impacts using a brain-spinal cord complex FE model. *Stapp Car Crash J.* 50, 509–44.
- KLEIVEN, S., HARDY, W.H., 2002. Correlation of an FE model of the human head with local brain motion-consequences for injury prediction. *Stapp Car Crash J.* 46.
- LI, J., ZHANG, J., YOGANANDAN, N., PINTAR, F., GENNARELLI, T., 2007. Regional brain strains and role of falx in lateral impact-induced head rotational acceleration. *Biomed. Sci. Instrum.* 43, 24–9.
- MARGULIES, S.S., THIBAUT, L.E., GENNARELLI, T. a, 1990. Physical model simulations of brain injury in the primate. *J. Biomech.* 23, 823–36.
- OBERKAMPF, W., TRUCANO, T., HIRSCH, C., 2004. Verification, validation, and predictive capability in computational engineering and physics. *Appl. Mech. Rev.* 57, 345–384.
- ROBERTS, J., HARRIGAN, T.P., WARD, E.E., TAYLOR, T.M., ANNETT, M.S., MERKLE, A.C., 2012. Human head-neck computational model for assessing blast injury. *J. Biomech.* 45, 2899–906.
- TAKHOUNTS, E.G., EPPINGER, R.H., CAMPBELL, J.Q., TANNOUS, R.E., POWER, E.D., SHOOK, L.S., 2003. On the Development of the SIMon Finite Element Head Model. *Stapp Car Crash J.* 47, 107–33.
- TAKHOUNTS, E.G., RIDELLA, S., HASIJA, V., 2008. Investigation of traumatic brain injuries using the next generation of simulated injury monitor (SIMon) finite element head model. *Stapp Car Crash J.* 52, 1–31.

- VAN NOORT, R., BLACK, M.M., MARTIN, T.R., MEANLEY, S., 1981. A study of the uniaxial mechanical properties of human dura mater preserved in glycerol. *Biomaterials* 2, 41–5.
- YANG, K., MAO, H., WAGNER, C., ZHU, F., 2011. Modeling of the brain for injury prevention. In: Bilston, L.E. (Ed.), *Neural Tissue Biomechanics. Studies in Mechanobiology, Tissue Engineering and Biomaterials*, pp. 69–120.
- YOGANANDAN, N., LI, J., ZHANG, J., PINTAR, F., 2009. Role of Falx on Brain Stress-Strain Responses. In: *Mechanosensitivity of the Nervous System*. pp. 281–297.
- ZHANG, L., YANG, K.H., DWARAMPUDI, R., 2001. Recent advances in brain injury research: a new human head model development and validation. *Stapp Car Crash J.* 45.